IJNRD.ORG ISSN : 2456-4184
INTERNATIONAL JOURNAL OF NOVEL RESEARCH AND DEVELOPMENT (IJNRD) | IJNRD.ORG
An International Open Access, Peer-reviewed, Refereed Journal

ADVANCED CONTROLLER FOR ENHANCING GRID-CONNECTED DOUBLY FED INDUCTION GENERATOR (DFIG)-BASED WIND ENERGY CONVERSION SYSTEM

[1]M Manikandan, [2]CH. Srikanth, [3]P. Keerthana, [4]A. Layasri, [5]M. Anusha

[1]Professor, [2,3,4,5]UG Students
[1,2,3,4,5]Department of EEE
[1,2,3,4,5]Jyothishmathi Institute of Technology and Science, Nustulapur, Karimnagar, TS, India

Abstract: In renewable energy power system is most popular in recent decades. In wind energy system, the power management capability, speed control operation, low converter cost and minimized energy losses are problem statement of the project. Firstly, an Artificial Neural Networks (ANN) has been introduced to give better dynamic performance during the fluctuating wind speed by keeping the output voltage stable. Secondly, The Neuro Fuzzy controller NFC is developed based on adaptive-network-based fuzzy inference system (ANFIS) for load side converter control. It improves dynamic performance under variable wind speed and load conditions by maintaining stable output voltage. In addition to that, the grid side harmonic is also minimized by implementing these methods. The performances have been tested on a 1.5 MW doubly fed induction generator (DFIG). The simulation results evident to the performance of ANN and ANFIS of Grid-Connected Doubly Fed Induction Generator (DFIG)-Based Wind Energy Conversion System using MATLAB simulation. The result of the Total Harmonic Distortion (%THD) is reduced for PI, ANN and ANFIS like 24.49%, 4.2% and 0.85% respectively.

IndexTerms **- Wind turbine system controllers, double fed induction generators, ANN, ANFIS, THD.**

I. INTRODUCTION

The wind power industry is seeing a rise in the adoption of DFIGs, or double fed induction generators, due to their several advantages over competing designs. Power from the rotor converter system makes up around a quarter up to the most output of a wind turbine, as stated by Malik et al. (2021). Induction machines' nonlinearity, dependency, and several variables make their control a formidable problem. Not all linear controller systems were equally successful, according to research by Tamalouzt et al. (2021). This included power-torque direct control, voltage-field-oriented control, and the proportional-integral-predictive (PID) controller. Wind turbine performance governed by DFIG has been the subject of much research on nonlinear controllers. Gupta and Shukla (2022) propose an optimal allocation of reactive power between machine and grid converters to enhance the DFIG. Beltran-Pulido et al. (2018) developed the present control rule to enhance the ridethrough low voltage by means of an active disturbance rejection control that possesses great robustness characteristics. To enhance the efficiency of the power conversion system and synchronize the grids, Xiong et al. (2019) looked into a coordinated super-twisting sliding mode control. A new sliding modecontrol based on the exponential reaching rule is presented by Liu et al. (2018) to decrease system chattering and accelerate the approaching process. The potential benefits of a multi-objective particle swarm optimization strategy for ride-through low voltage in improving dynamic stability in the presence of electrical disturbances were explored by Aguilar et al. (2020). But advanced nonlinear controllers are required for the DFIG-based wind energy converter to operate better. Since its start in the 1970s, model predictive control (MPC) has made great strides (Mahmoud and Oyedeji, 2019). Possible topics covered include predictive functional control, algorithmic model control, adaptive control with an enlarged horizon, (Nosratabadi et al., 2019). A plant model, which is a kind of feedback control, allows the MPC to predict the plant's outputs over a certain time frame. With these constraints and these predictions, determining the best control is as simple as solving an optimization problem (Schwenzer et al., 2021). By employing a nonlinear observer variation of an adaptive second-order sliding algorithm, the conversion system is optimized, efficiently, and reliably executed (Zhang et al., 2019a). This algorithm has been fine-tuned specific features and control requirements of different kinds of variable-speed wind turbines in mind. By analyzing the nonlinear MPC's performance under various wind conditions with a fixed coefficient of static drag, a fuzzy regulator can be built to modify the weight coefficient of the cost function. For the purpose of maximizing energy harvesting and generator torque variation, Song et al. (2022b) provide a marine-optimized multi-objective predator algorithm. According to Zhang et al. (2019b), a DFIG wind system may be implemented to handle both balanced and

unbalanced network situations. We do this by using a simple and general method for predicting direct power management. An MPC capable of withstanding high-voltage ride through was built by Zhou et al. (2021) using P-Q coordination. Song et al. (2022a) offer the SMPYC technique, which is based on intelligent scenario generation (ISG). In order to prove that wind direction projections are inherently inaccurate, the ISG method suggests making scenarios. Then, by implementing the proposed SMPYC that is scenario-based to improve the yaw action, the energy collecting efficiency of WTs is increased. A dizzying array of mechanical sensorless control techniques are available for induction devices. The use of an ANN was shown by Tamalouzt et al. (2022) to control the direct torque of a dual power induction motor. As an alternative to a physical sensor, the Kalman filter that is extended may act as an observer in this method. By combining an adaptive flux and speed observer-based method with an adaptive system estimator that depends on a model reference, Researchers Tamalouzt et al. (2022) made sure that the speed of the rotor in a five-phase induction motor estimate was accurate. A controller-robust strategy for wind energy conversion systems that assess the aerodynamic force is proposed by Ouari et al., 2014a. This approach combines a disturbance observer with a nonlinear generalized predictive control. Using a sliding mode approach of second order, El Daoudi et al. (2021) develop a load torque observer for induction motor drives. Creating a new trustworthy controller capable of optimizing wind energy absorption autonomously, without requiring human intervention or data on aerodynamic torque. Enhancing the system can be achieved, for example, by making adjustments to the conventional NGPC cost function that uses Taylor series expansion. By all accounts, the nonlinear predictive controller is working very hard. By maintaining stability within the face with settings that aren't compatible and unknown disturbances, proposed controller eliminates the steady-state error totally in the closed-loop system. When pinpointing the output's mistake converges to its source, we say that the locked system is stable. Following the control's activation, we validated its trajectory and perturbation rejection using simulations.

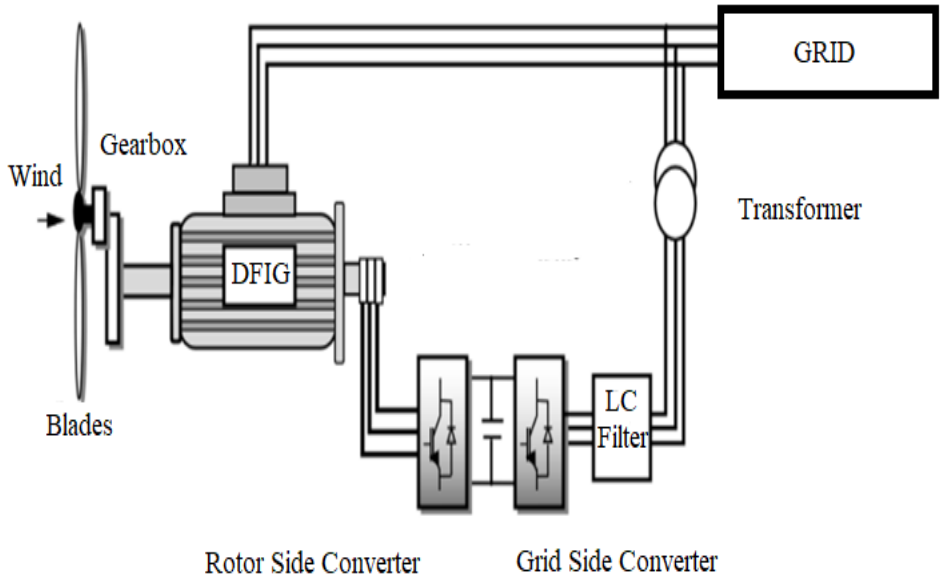

Figure 1. Schematic Diagram of the DFIG wind turbine system.

Figure 1 shows a schematic of the DFIG wind turbine arrangement. The AC-DC-AC converter provides the rotor with variable-frequency power, while the stator remains permanently linked to the three-phase power grid (Tamalouzt et al., 2021).

DFIG wind turbine system description and energy conversion

The technology behind DFIG wind turbines is shown in Figure 1. An AC-DC-AC converter supplies the rotor with varying frequencies, while the stator is hardwired into the three-phase power grid (Tamalouzt et al., 2021).

II. LITERATURE SURVEY

Reducing flicker emissions energy produced by wind turbines linked to the grid has been the focus of several strategies. Reactive power adjustment is widely used. Flicker reduction has its limits when used to distribution networks with low grid impedance angles. In the event of a high wind speed and a grid impedance angle of 10 degrees, flickering cannot occur until 3.26 watts of reactive power are supplied per unit. Each doubly fed induction generator (DFIG) unit has a converter capacity of around 0.3 kW, which makes it extremely challenging for grid-side converters (GSCs) to produce reactive power of this type. The use of the well-known STATCOM effectively reduces flicker output. It is quite unlikely that applications involving distributed generation would be cost-effective. One way to reduce flicker emission is by active power regulation, which involves changing the back-to-back converter's dc-link voltage [8]. While this option does require a large rectifier capacitor to stabilize the changing power of the dc connection, its lifespan is significantly shorter compared to the others.

Flicker emission at high wind speeds is studied using an open-loop pitch control, disregarding the pitch actuation system (PAS). Because of their significant impact on the emission of flicker results of variable-speed wind turbines, the pitch rate and time delay of the PAS must be carefully considered.

Instead of using the pitch actuation system (PAS), researchers can use an open-loop pitch control to study flicker emission in high wind conditions. Because they affect the flicker emission outcomes, the pitch rate and time delay of the PAS are important design issues for variable-speed wind turbines.

One innovative approach that has the potential to lessen workloads is the use of in-process control (IPC). There is minimal impact on electrical power when structural loads are reduced with the IPC. Instead, this study recommends reducing flicker in grid-connected wind turbines using an IPC technique. A simple way to eliminate flicker is to align the proposal angles of the wind turbine and generator. This will reduce voltage changes by dampening power oscillations. Flicker emission's effect on the structural load is also considered. The concepts of fatigue, aerodynamics, structures, and turbulence may be used to build a example of a three-bladed wind turbine.

The grid is unaffected by operating a rotor with changing speed since the flywheel is designed to absorb and lessen unexpected power spikes. As an added bonus, this significantly reduces grid electrical flicker. The flickering noise from wind turbines that are linked to the power grid employing DFIG is a key motivation for doing this research. Because of this, adding more wind power production to the existing system will be less of a hassle. Due to the growing importance of wind power as a grid power source, especially in times of emergency like voltage dips or difficulties with short circuits, research into the interplay between wind turbines and the grid is essential. Wind power is constantly increasing its penetration into the grid, and system operators are ensuring its stability and electricity supply by setting guidelines for grid integration. If there is an external grid short circuit, the terminal voltages of wind turbines must return to their original values as soon as the fault is cleared, according to Danish standard. The electricity will remain on even if the wind turbines are not in use. German, Dutch, English, and Welsh standards are on par with international ones. Turning down a large amount of wind power during periods of high wind penetration is not a wise decision from a safety standpoint. This might put the dependability of the power grid at risk if put into action. Among the many critical issues that must be addressed by this analysis of wind turbines that are linked to the power grid is the matter of voltage recovery following an external short-circuit repair.

III. PROPOSED SYSTEM

The following formula is employed to ascertain the mechanical power of the wind because wind turbines have a poor conversion efficiency (Soliman et al., 2021; Belkhier et al., 2022).

$$P_t = \frac{1}{2}\rho_a \pi R^2 C_p(\lambda, \beta) v^2 \quad (1)$$

uses the speed ratio λ and the blade pitch angle β to determine the power coefficient Cp(λ, β) of the turbine: To find the amount of wind energy that has been gathered, Pt, we multiply the air density (ρa), the blade radius (m), and the wind speed (v).

$$C_p(\beta, \lambda) = (0.3 - 0.0167\beta)\, sin\left(\frac{\pi(\lambda + 0.1)}{10 - 0.3\beta}\right) - 0.00184(\lambda - 3)\beta \quad (2)$$

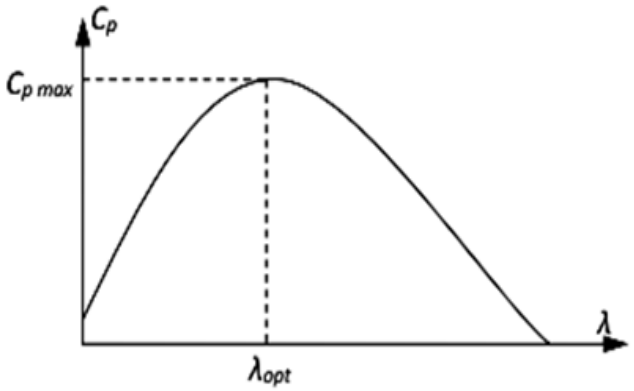

Figure 3.A. Power Coefficient

We may find the tip-speed ratio λ of the blade using this method:

$$\lambda = \frac{\Omega_t R}{v} \quad (3)$$

To convert the maximum amount of wind power, the generator's power characteristic should align with the maximum Cp−max line, as seen in Figure 3.A. The highest value of the power coefficient Cp is 0.55006, assuming a speed ratio of 8 and a blade pitch angle of 0°. Decreased reactive power to zero allowed for a power factor of one. Maximum power point tracking (MPPT) was used to calculate the rotor speed and active power references of the control block, as stated by Belkhier et al. (2022).

$$\begin{cases} P_{grid-ref} = \frac{1}{2}\rho_a \pi R^2 C_{p-max} v^3 \\ \Omega_{r-ref} = \frac{\lambda_{opt}}{R} v \end{cases} \quad (4)$$

Several parameters should be included in the variables Ωr−ref, Λopt, Cp−max, and Pgrid−ref in the previous equation. These elements include the active power reference of the electrical grid, the reference rotor speed, the optimal speed ratio, and the upper power coefficient.

Ihari with his colleagues at work.

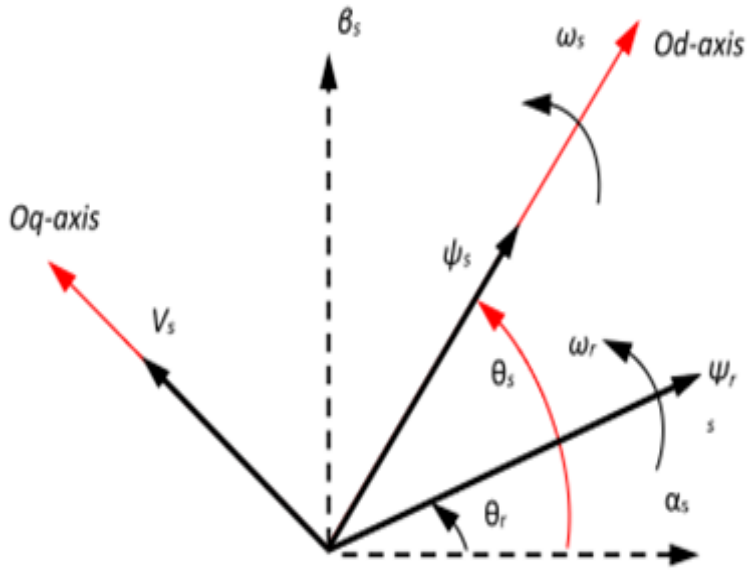

Figure 3.B. Voltage and Flux Vector Settings

3.1 VSC designing:

Reducing switching losses and increasing power extraction are the primary objectives of VSC design. The controls of conventional converters are intuitive due to their simple design. To evaluate duty cycle ratios with present VSCs, PWM methods are too complicated and unpredictable. Consequently, these VSCs can end up having very high operating and maintenance costs. Using these converters in tandem with cost-optimized operations and predictive control solves this problem.

As an illustration, the leg voltage of a power converter may be

$$V_{xn} = S_x - S_y . V_{dc} \quad x=y=a,b,c \quad (5)$$

$$V_0 = V_{xn} - R_{eq} . I_o - L . \frac{dio}{dt} \quad (6)$$

The following voltage and current vector representations are necessary to show how the circuit model operates in figure 2:

$$V_{pul} = [V_R \; V_Y V_B]^T \quad (7)$$

V_{Pwm}= 3ph inv o/p to neutral line voltages

$$I_i = [I_R \; I_Y I_B]^T \quad (8)$$

$$V_l = [V_R \; V_Y \; V_B]^T \quad (9)$$

Equation from load view:

$$V_L = R_f I_{inv} + L_f \frac{dio}{dt} + V_{pwm} - R_n I_n - L_n \frac{din}{dt} \quad (10)$$

$$I_{inv} = I_L + C_f \frac{dVL}{dt} \quad (11)$$

3.2 The DFIG model

In Figure 3, the d-axis is aligned with the stator flow vector under the synchronous orientation frame, the following state equations build the DFIG model, ignoring the stator resistance.

$$\begin{cases} x(t) = f(x) + B(x)u(t) \\ y_i(t) = h_i(x) i = 1, \dots, m \end{cases} \quad (12)$$

$$\begin{cases} \dfrac{di_{dr}}{dt} = -\dfrac{R_r}{\sigma L_r} i_{dr} + s\omega_s i_{qr} + \dfrac{1}{\sigma L_r} V_{dr} \\ \dfrac{di_{qr}}{dt} = -\dfrac{R_r}{\sigma L_r} i_{qr} - s\omega_s i_{dr} + s\dfrac{MV_s}{\sigma L_r L_s} + \dfrac{1}{\sigma L_r} V_{qr} \end{cases} \quad (13)$$

as soon as σ 1 transforms into M2. The given sequence for the dqrotor's current and voltage consists of the variables Vdr, Vqr, idr, and iqr. Rr is the resistance of the rotor winding and Lr is the inductance of the rotor. The angular velocities of the rotor are denoted by ór and those of the stator by ós in this context. The letters s and σ represent the generator slip and dispersion ratios, respectively. Considering the rotor's angle (dq-axis) with respect to the Park reference allows for the adjustment of rotor quantities in a Park approach. The potential formula for this angle is μ μs − μr, where ör is the angular rotor's speed, Ωr is the mechanical rotor's speed,

P is the number of poles, fs is the grid's frequency, and ϋs = 2π fs, θrórdt, and □s χsdt. Here is an alternative way to show the generator's torque:

$$T_{em} = P\frac{M}{\omega_s}\frac{V_s}{L}i_{qr} \qquad (14)$$

Here are several formulae that can help you find the active and reactive stator powers:

$$\begin{cases} P_s = -\dfrac{M}{L_s}V_s I_{qr} \\ Q_s = \dfrac{V_s^2}{\omega_s L_s} - \dfrac{M}{L_s}V_s I_{dr} \end{cases} \qquad (15)$$

The mechanical equation is

$$J\frac{d\Omega_r}{dt} = T_{em} - T_r - f_r\Omega_r \qquad (16)$$

Tr, fr, J, and Tem are all variables that pertain to turbines. Total inertia, electromagnetic torque, total external damping, and aerodynamic torque after the gearbox are some of these factors.

3.3 Ruby nonlinear generalized predictive control proposed

Tr, fr, J, and Tem are all variables that pertain to turbines. Total inertia, electromagnetic torque, total external damping, and aerodynamic torque after the gearbox are some of these factors.

$$\Im(x,u) = \int_0^t [y_r(t+\delta) - y(t+\delta)]^T [y_r(t+\delta) - y(t+\delta)]\, d\delta \qquad (17)$$

This study proposes a robust nonlinear generalized predictive control (RNGPC) as a potential solution to the robust control problem by modifying the traditional cost function (9). Take into account the multi-variable nonlinear system:

$$\begin{cases} \dot{x}(t) = f(x) + B(x)u(t) \\ y_i(t) = h_i(x) i = 1, \dots, m \end{cases} \qquad (18)$$

where the members of the set Rn are the state vector (x) and the control vector (u). Given that f(x) and h(x) are continuously differentiable, we may express B(x) as a function of x. Finding the optimal value of the new cost function I(x,u) to minimize will maximize the effectiveness of the predictive command.

$$\Im(x,u) = \frac{1}{2}r(t+\tau)^T r(t+\tau) \qquad (19)$$

$$\text{r(t)} = \int_0^t [y_r(\delta) - y(\delta)]d\delta \qquad (20)$$

3.4 Electromagnetic torque and current predictive control

By utilizing the speed controller (outer loop) to calculate the d-axis rotor current reference and derive the electromagnetic torque reference, the reactive power of the DFIG may be kept at zero. Using Equation (5) as a matrix, we may express the electrical equations as follows:

$$\begin{cases} \dot{x}(t) = f(x) + g_u(x)u(t) \\ y = h(x) \end{cases} \qquad (21)$$

With $x = (i_{dr} i_{qr})^T, u = (V_{dr-ref} V_{qr-ref})^T, and\ u = (T_{em} i_{dr})^T$

$$\text{f(x)} = \begin{pmatrix} -\frac{R_r}{\sigma L_r} i_{dr} + s\omega_s i_{qr} \\ -\frac{R_r}{\sigma L_r} i_{dr} - s\omega_s i_{dr} + s\frac{V_s}{\sigma L_r L_s} \end{pmatrix} and\ g_u(x)$$

$$= \begin{pmatrix} \frac{1}{\sigma L_r} & 0 \\ 0 & \frac{1}{\sigma L_r} \end{pmatrix}$$

The subsequent outputs will be controlled by the inner loop:

$$\begin{cases} y_1 = h_1(x) = T_{em} = P\dfrac{MV_s}{\omega_s L_s} i_{qr} \\ y_2 = h_2(x) = i_{dr} \end{cases} \qquad (22)$$

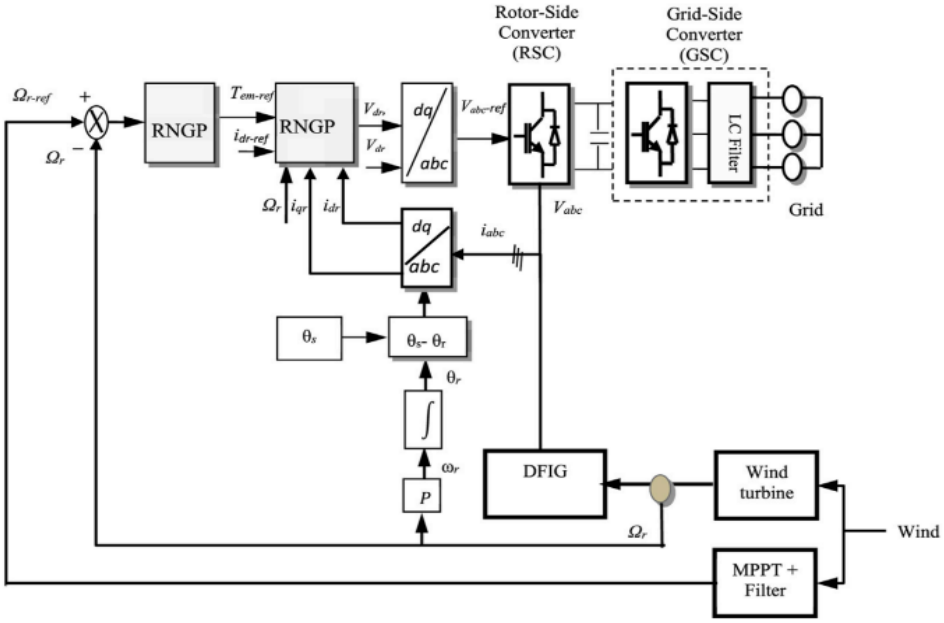

Figure 3.C. Block Diagram of the proposed ANN with grid.

IV. CONTROLLERS THAT USE FUZZY LOGIC AND NEURAL NETWORKS

Instead of using a fuzzy controller, a neural network regulator is taking over, and it will be able to govern the rotors as well as the grid. The NNF Tool neural network fitting tool in MATLAB accomplishes this learning objective by utilizing the Levenberg-Marquardt propagation approach. The output layer has now communicated the error to the input layer. To do this, you need to tweak the NN (Neural Network) weights until you achieve the learning coefficient that you wish. Ideally, it should be 0.93 or higher. The objective is to discover a structure that outperforms the competition in terms of hidden layer density and neuron density per layer. Due of this, a number of studies have sought to identify the optimal network design. A three-layer neural network with an input, hidden, and output layer is the best design. The activation was performed using a sigmoid function.

$$X^{(1)}(k) = [W^{(1)}(k)]^T . X(k)$$
$$O^{(1)}(k) = f^{(1)}\left(X^1(k)\right)$$
$$X^{(2)}(k) = \left[W^{(2)}(k)\right]^T O^{(1)}(k)$$
$$O^{(2)}(k) = f^{(2)}(X^{(2)}(k))$$
$$\mathrm{Y(k)} = O^{(2)}(k)$$

As an input vector, X (k), has a size of (m ¼ 1). Both the hidden and output layers contain weight matrices, with the former including W(1)(k) and the latter W(2)(k). Clearly, the first matrix has dimensions of (m n) ¼ (1 3) while the second matrix has dimensions of (n p) ¼ (3 1), respectively. The input vector of the hidden layer is denoted as and its output vector is assuming an output layer size of (n 1) ¼ (3 1) and (p 1) ¼ (1 1) respectively.

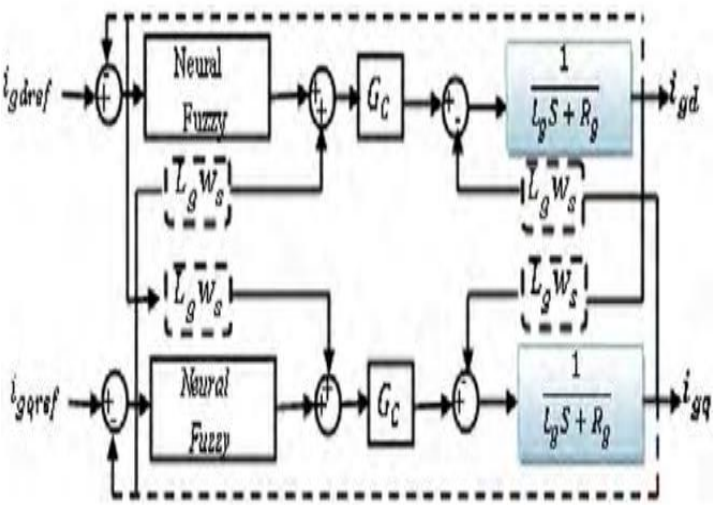

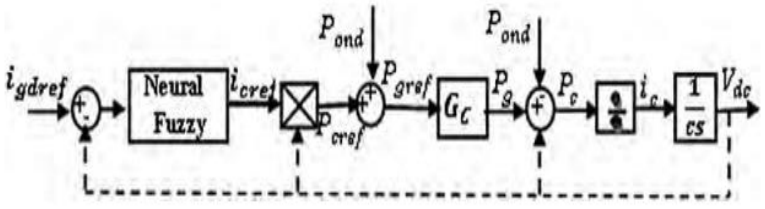

Fig. 7. Control loop of the DClink voltage.

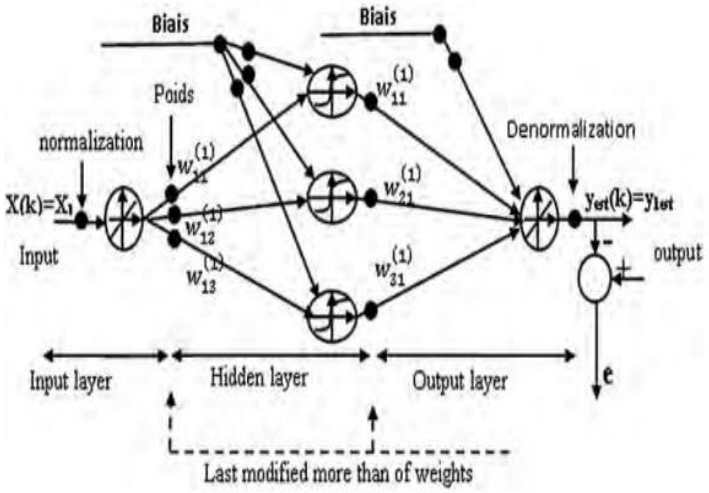

Figure 4. A single-hidden-layer neural network architecture

V. SIMULATION RESULTS

When DFIG receives a, it maximizes conversion efficiency by adjusting its active power to be almost identical to its reference. It is evident that the grid power factor has been rectified when the DFIG reactive power remains zero. Synchronous (s = 0), hyper-synchronous (s < 0), and sub-synchronous (s > 0) are the three ways the rotor voltage-current is shown. These sorts of outcomes demonstrate the efficacy of the suggested RNGPC method in both static and dynamic contexts.

For illustration purposes, the DFIG model makes use of the following parameter values: Both the friction coefficient at time 7 s and the rotor's resistance at time 10 s are affected by this problem, although to varying degrees. The effectiveness of the controller is also assessed in this test by varying the prediction horizon. All prediction horizons, with the exception of the outer loop Tp2, have seen a decrease from 15 ms to 1.5 ms. It is sad that the controller is totally oblivious to this variance. The response of the system converges to the reference values regardless of how unexpected the DFIG parameters are. When it comes to electromagnetic torque and speed, they both follow their corresponding tee references to the letter. Reduced control effort thanks to the speed filter allows for shorter prediction horizons and quicker disturbance rejection.

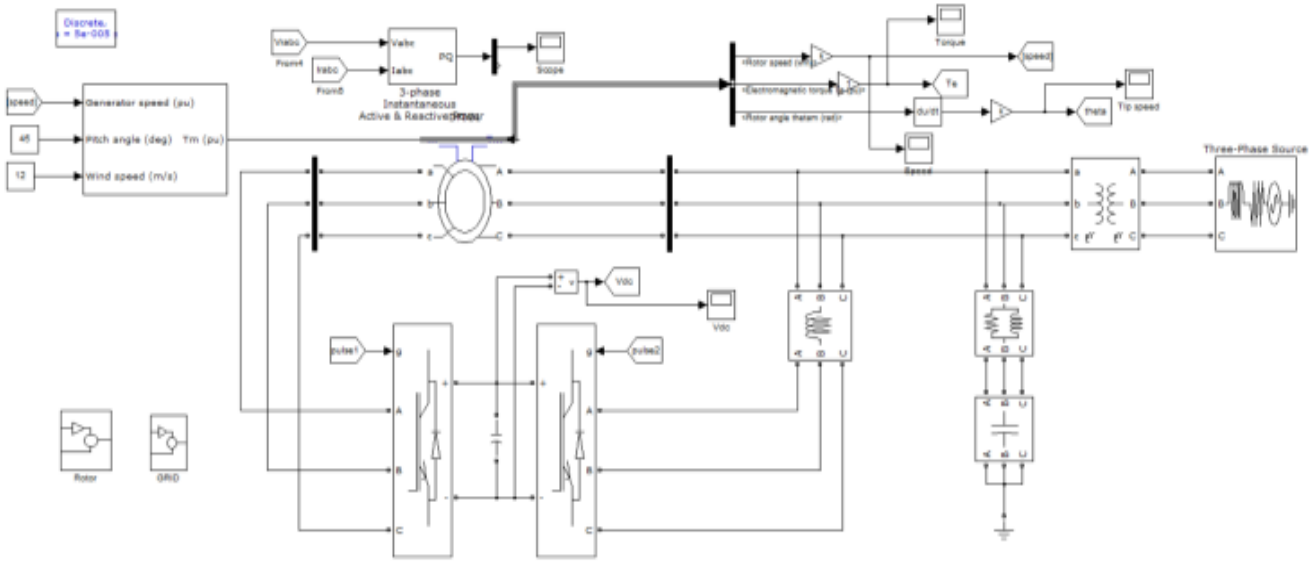

Fig 5. Simulation circuit model of DFIG based wind system.

The above figure 5. shows the simulation model that we used in this DFIG based wind system. In this simulation we used back-to-back converters for the rotor side and grid side respectively.

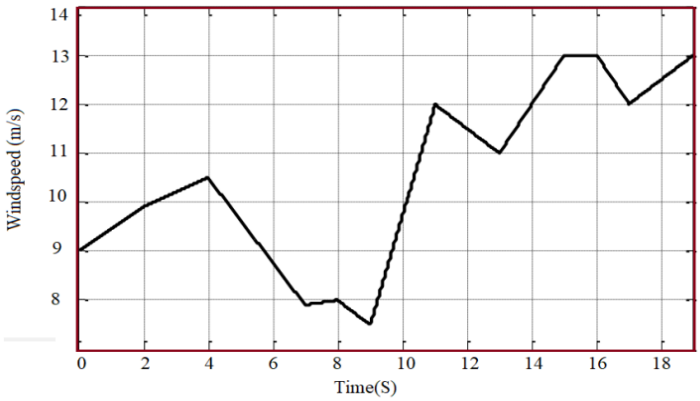

Figure 6. Wind speed Profile.

The above graph (figure 6.) shows the rate of wind speed profile ratio. We can observe that wind speed is not constant throughout the given time. It varies with respect to the time. At initial it is medium speed, then it fallen to below 8 m/s at the range of 9 seconds and then suddenly it continuous to raise and reaches to maximum point.

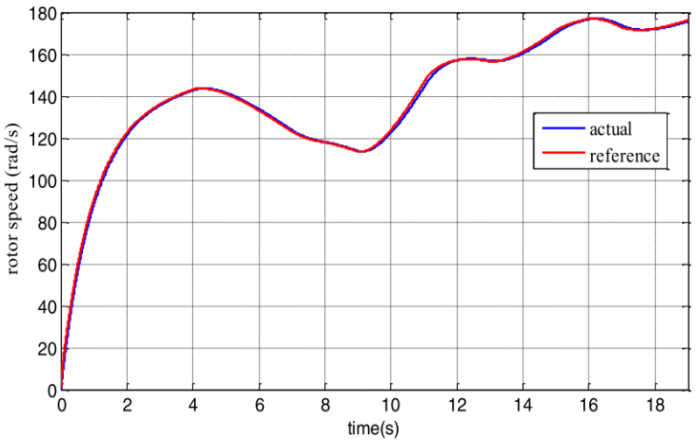

Figure 7. Rotor Speed Response

The figure 7. Shows the curve of rotor speed responses of both the actual rotor speed and reference rotor speed. It seems to be be same for both the responses.

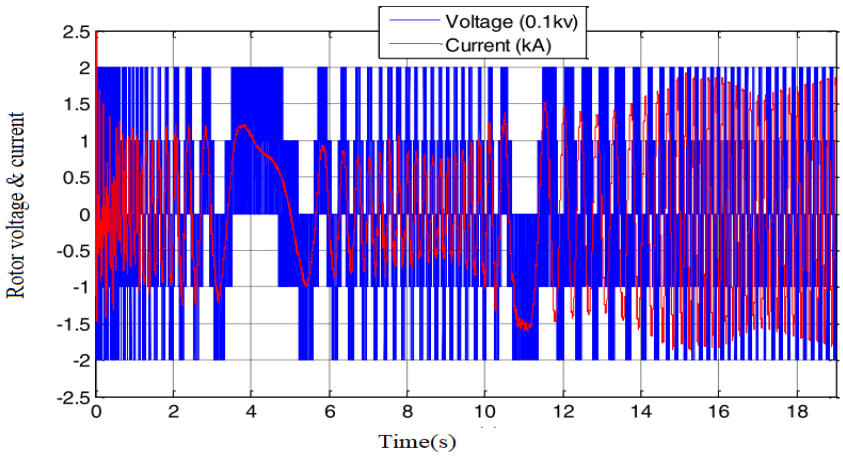

Figure 8. Rotor voltage and Current.

The above waveforms in figure 8. is representing the voltage and current of rotor. Here all the quantities are considered in the terms of per unit system values. Voltage is taken as 0.1kv and current in kA in each unit.

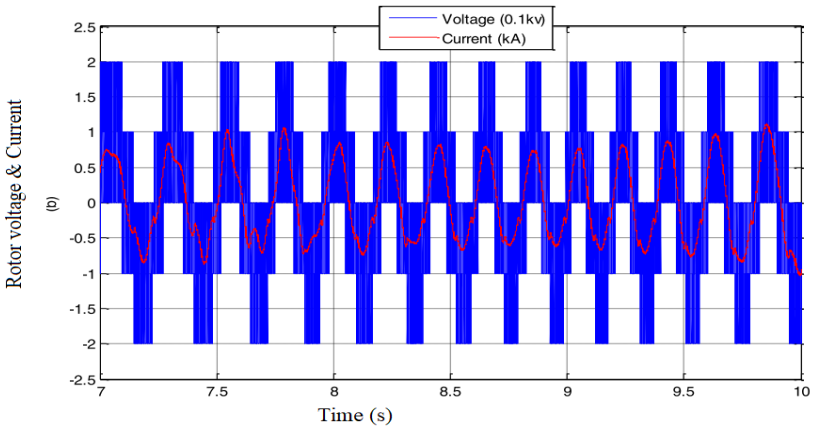

Figure 9. Sub Synchronous mode of rotor voltage and current.

The above figure 9. Shows sub synchronous mode of rotor voltage and current in the given time. It allows utilization of wind power at lower wind speed.

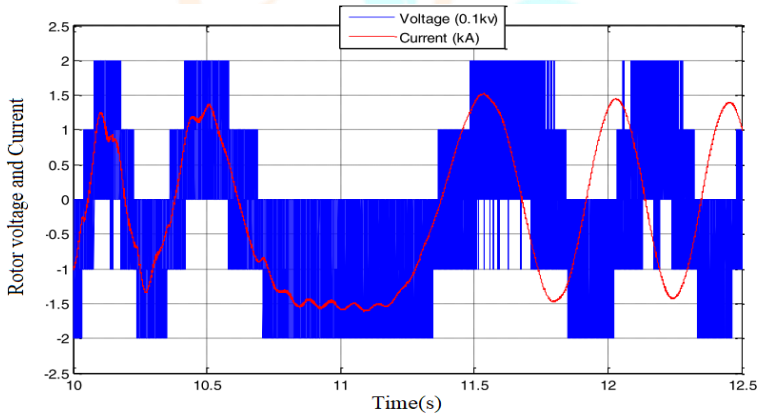

Figure 10. Synchronous mode of rotor voltage and current.

The above figure 10. Shows the synchronous mode of rotor voltage and current which is directly provided by the dc capacitor. We can observe that at initial there is some disturbances in the current and then after a while it becomes normal. Similar with the voltage also.

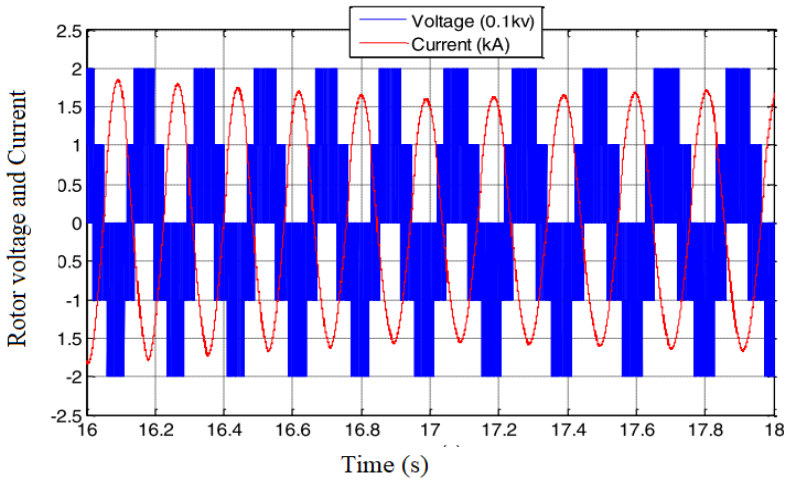

Figure 11. Super Synchronous mode of rotor voltage and current.

The above figure 11. Shows about the super synchronous mode of rotor voltage and current. In this mode the rotor voltage and current are returned to AC system but with different phase sequences.

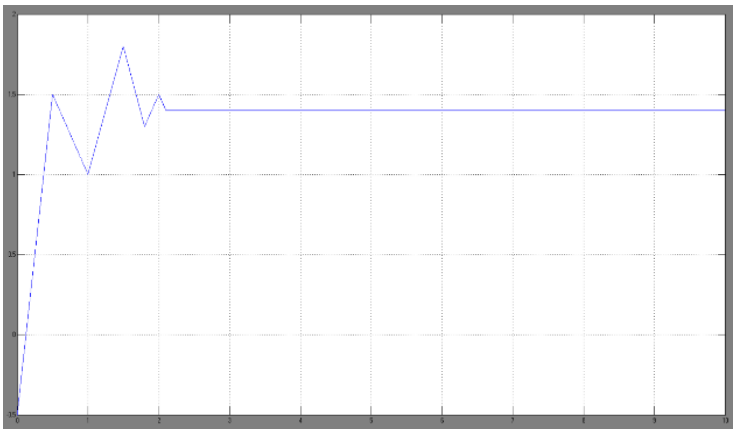

Figure 12. Rotor speed vs time graph

Figure 12 shows the graph of rotor speed vs time. In this we taken reference point from the -15 to 2 through y-axis and 0 to 10 in the x-axis. It shows at starting the rotor speed is not constant, it is fluctuating and then after a sometime it becomes constant throughout the time.

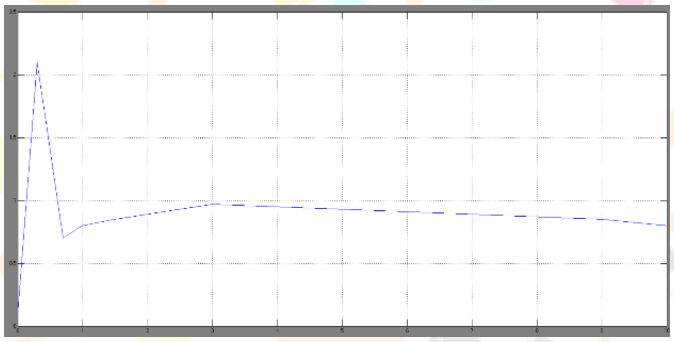

Figure 13. Torque vs time graph.

Figure 13 shows the graph of a torque vs time curve. Y-axis is torque from 0 to 2 with each unit as 0.5 N-m and X-axis is time from 0 to 10 micro sec. The torque is almost assumed like constant and slightly decreases as speed is constant. But in starting it starts from 0 and reaches to maximum point, it can be seen more compared to final point.

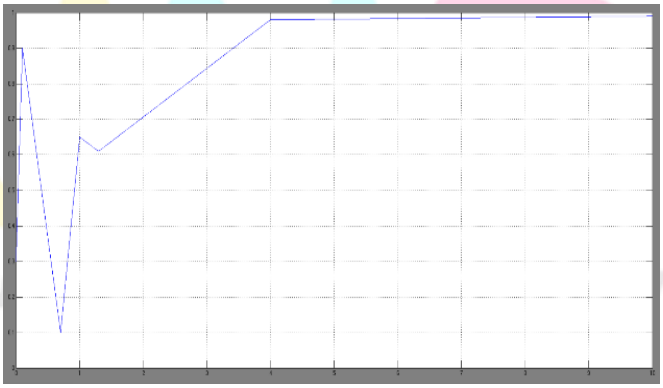

Figure 14. Power vs time graph injected to grid.

The above figure 14 shows the graph of power vs time which is injected to grid. Initially the power delivered to the grid is not constant and then with a particular duration of time it is delivered as constant by eliminating the distortions in it using the advanced controlling methods.

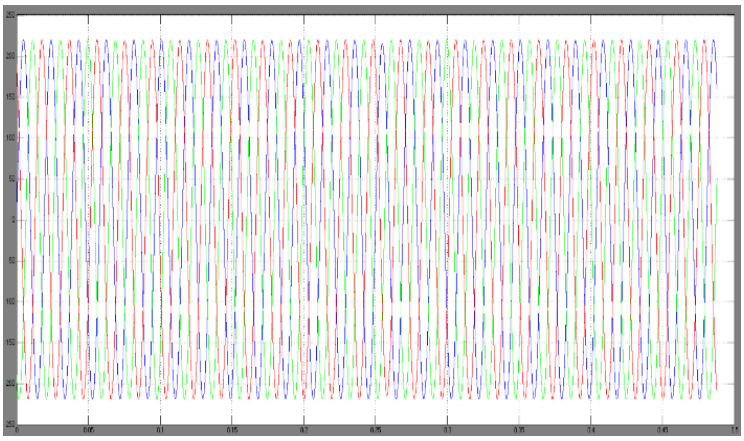

Figure 15. Grid voltage vs time.

In the above figure 15 grid vs voltage time shows the sinusoidal waveforms, reflecting the alternating current (AC) nature of the electricity grid. It is designed to operate at a specific grid frequency, which is typically 50 Hz or 60 Hz, depending on region ensuring the output voltage matches the grid voltage.

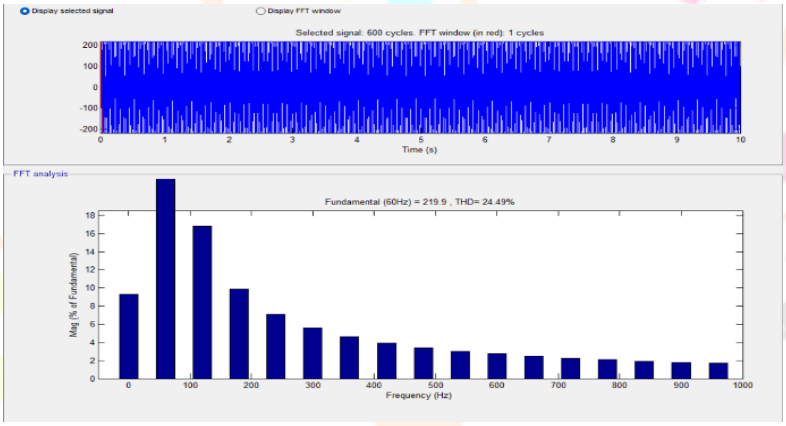

Figure 16. THD analysis of grid voltage with PI controller 24.49%

The above graph shows the analysis of grid voltage with PI controller. Here we have observed that by using the PI controller the Total Harmonic Distortion (THD) value is 24.49% , which is not good for power quality management.

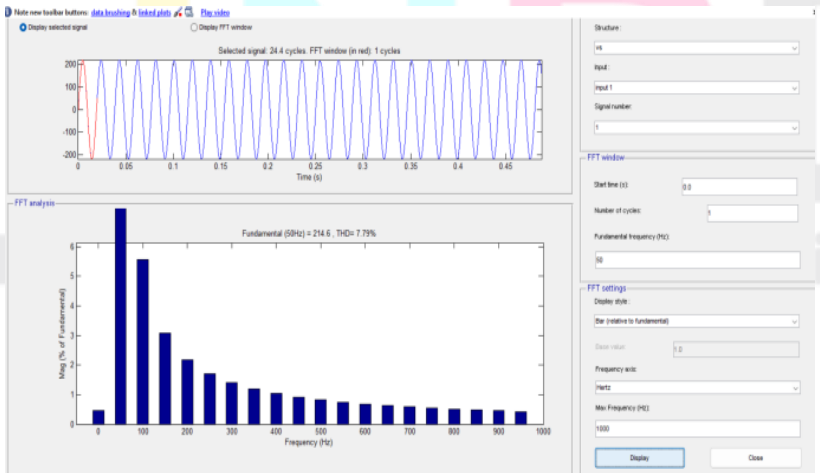

Figure 17. THD analysis of grid voltage ANN controller 7.79%

The above figure 17 is about the analysis of grid voltage using the Artificial Neural Network controller. In this analysis we have observed that the THD value is about 7.79% which means it is better approach than the PI controller. We can use this approach for DFIG wind energy system for better performance.

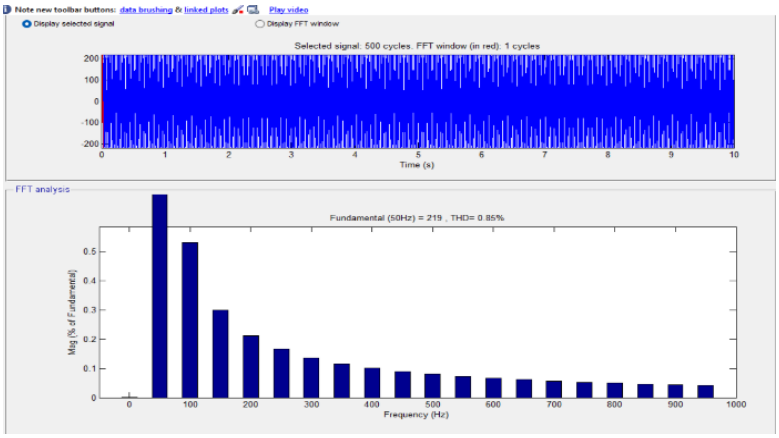

Fig.17. Thd analysis of grid voltage NEURO FUZZY controller 0.85%

The above figure 18 shows the analysis of grid voltage by using the NEURO FUZZY controller. It reveals that the total harmonic distortion value is about 0.85% which means that it is more suitable for wind energy utilization through the grid with good quality of power delivery.

Table 1. Comparative analysis table of grid voltage THD using different type of controllers.

Controller	**THD %**
PI	**24.49%**
ANN	**7.79%**
Neuro fuzzy	**0.85%**

The above table 1 gives the comparison among the three approaches used in this work. It is cleared that by using different controllers we will get different THD values and by using the modern advanced control techniques like ANN and NEURO FUZZY we can get the THD as minimized level. Hence, it is better to use combined neuro fuzzy controller for better results.

VI. CONCLUSION

Using fuzzy logic controllers and neural networks, this research introduces a new control mechanism for grid-connected DFIG-based WECS. To achieve control, one can utilize an electrical converter in conjunction with switching based on pulse-width modulation (PWM). In this electrical configuration, the WECS control mechanism may be programmed to provide fuzzy control over speed variation, enabling maximum power point extraction. An inverter for three-phase voltage, which controls this DC connection voltage, which is then used to re-inject the harvested electrical power into the grid. The findings indicate that the suggested controllers are successfully regulating the system's operation. There is an obvious connection between the measured powers and the new reference when the wind speed changes. Since it makes use of effective neural networks and fuzzy logic controllers, the suggested framework may be a good substitute for DFIG wind turbine wind energy conversion systems, according to the findings.

This work has resulted in a reliable generalized predictive controller that is nonlinear and designed for use with DFIG wind turbine systems. Because the control method is robust against changes in both parameters and aerodynamic torque, an observer of aerodynamic torque is unnecessary. This is due to the program's unique finite horizon cost function. Wind power would be ideal in that region if the amount of active electricity transmitted to the grid could be influenced by the speed of the wind. The control architecture can resist unknown aerodynamic torques, according to the simulation findings. That the planned control consistently cites the anticipated sources is established beyond a shadow of a doubt. The efficiency and dependability of the RNGPC were validated by the outcomes of the simulations run under various operational circumstances and with varying values for the DFIG parameters.

ACKNOWLEDGEMENT AND FUNDING

The authors receive no financial support for the research, authorship, and publication of this article.

DECLARATION OF CONFLICTING INTERESTS

The authors declare no potential conflicts of interest with respect to the research and publication of this article.

REFERENCES

[1] Aguilar, M. E. B., Coury, D. V., Reginatto, R., and Monaro, R. M. (2020). Multi-objective PSO applied to PI control of DFIG wind turbine under electrical fault conditions. Electr. Power Syst. Res. 180, 106081. doi:10.1016/ j.epsr.2019.106081

[2] Belkhier, Y., Achour, A., Ullah, N., and Shaw, R. N. (2022). Modified passivitybased current controller design of permanent magnet synchronous generator for wind conversion system. Int. J. Model. Simul. 42 (2), 192–202. doi:10.1080/ 02286203.2020.1858226

[3] Beltran-Pulido, A., Cortes-Romero, J., and Coral-Enriquez, H. (2018). Robust active disturbance rejection control for LVRT capability enhancement of DFIGbased wind turbines. Control Eng. Pract. 77, 174–189. doi:10.1016/j.conengprac. 2018.06.001 El

[4] Daoudi, S., Lazrak, L., El Ouanjli, N., and AitLafkih, M. (2021). Applying sliding mode technique for the nonlinear DTC-SPWM control strategy of sensorless squirrel cage asynchronous motor. Int. J. Dyn. Control 9 (4), 1633–1644. doi:10. 1007/s40435-021-00758-8

[5] Evangelista, C. A., Pisano, A., Puleston, P., and Usai, E. (2016). Receding horizon adaptive second-order sliding mode control for doubly-fed induction generator based wind turbine. IEEE Trans. Control Syst. Technol. 25 (1), 73–84. doi:10.1109/ tcst.2016.2540539

[6] Gupta, S., and Shukla, A. (2022). Improved dynamic modelling of DFIG driven wind turbine with algorithm for optimal sharing of reactive power between converters. Sustain. Energy Technol. Assessments 51, 101961. doi:10.1016/j.seta. 2022.101961

[7] Liu Y., Wang, Z., Xiong, L., Wang, J., Jiang, X., Bai, G., et al. (2018). DFIG wind turbine sliding mode control with exponential reaching law under variable wind speed. Int. J. Electr. Power & Energy Syst. 96, 253–260. doi:10.1016/j.ijepes.2017. 10.018

[8] Mahmoud, M. S., and Oyedeji, M. O. (2019). Adaptive and predictive control strategies for wind turbine systems: A survey. IEEE/CAA J. Autom. Sin. 6 (2), 364–378. doi:10.1109/jas.2019.1911375

[9] Malik, M. Z., Baloch, M. H., Gul, M., Kaloi, G. S., Chauhdary, S. T., and Memon, A. A. (2021). A research on conventional and modern algorithms for maximum power extraction from wind energy conversion system: A review. Environ. Sci. Pollut. Res. 28 (5), 5020–5035. doi:10.1007/s11356-020-11558-6

[10] Nosratabadi, S. M., Bornapour, M., and Gharaei, M. A. (2019). Grasshopper optimization algorithm for optimal load frequency control considering predictive functional modified PID controller in restructured multi-resource multi-area powerresilience are confirmed by simulation results under a variety of operating conditions and DFIG parameter variations.

[11] Manikandan Mani, Praveen Kumar Thota, Ganapathy Somaskandan (2024)Voltage Stability Analysis for Grid Connected PV System using Optimized Control on IOT based ANFIS, PRZEGLĄD ELEKTROTECHNICZNY 100. 259-266

[12] Ramesh, R., Sasi, C., & Manikandan, M. (2023). An Efficient PV - Integrated UPQC System for Power Quality Enhancement Using Improved Chicken Swarm Optimization. International Journal of Experimental Research and Review, 33, 57-70.

[13] Dr.Manikandan, P Balashan, Chidambram I.A (2023). An ANN Based MPPT for Power Monitoring in Smart Grid using Interleaved Boost Converter Tehnički Vjesnik - Technical Gazette, 30(2) (SCI)

[14] Dr.Manikandan, Abdul Quawi , Y. Mohamed Shuaibi (2023). Power Quality Improvement Using ANN Controller For Hybrid Power Distribution Systems, Intelligent Automation & Soft Computing, 36(3)

[15] Manikandan Mani, Ramesh Rudraram, Sasi Chinnathambi (2023), "A Novel Intelligent Neural Network Techniques of UPQC with Integrated Solar PV System for Power Quality Enhancement" International Journal of Electronics and Telecommunications, 2023, vol. 69, NO. 3, PP. 605-613.

[16] M Manikandan, Ch Sathish, IA Chidambaram, (2023) Switched Z-Source Boost Converter in Hybrid Renewable Energy System for Grid-Tied Applications, Journal of Electrical Systems, , Issue, 1 , vol 19,page 64-81.

[17] M Manikandan, Ch Sathish, I Chidambaram, , (2023), Hybrid Renewable Energy System with High Gain Modified Z-Source Boost Converter for Grid-Tied Applications, Problemele Energeticii Regionale, Issue 1 , vol 57,page 39-54. WOS-ESCI)- (Scopus)

[18] Manikandan Mani, Ramesh Rudraram, Sasi Chinnathambi (2023), PV Integrated UPQC with Intelligent Control Techniques for Power Quality Enhancement, International Journal of Electrical and Electronics Research (IJEER), Issue 1 , vol 11, page 202-212.

[19] Manikandan Mani, Praveen Kumar Thota, Ganapathy Somaskandan (2023), The Voltage stability analysis for grid-connected PV system using optimized control tested by IEEE 14 &30 bus system, International Journal of Experimental Research and Review, , Issue 3 , vol 30. Page 09-118

[20] Dr.Manikandan, Sathish Ch, Chidambram I.A., Intelligent cascaded adaptive neuro fuzzy interface system controller fed KY converter for hybrid energy based microgrid applications (Jan 04, 2023). Electrical Engineering & Electromechanics, (1) 63–70, 2023.

[21] Dr.Manikandan, M, P. Balakishan. and I. A. Chidambaram., Improvement of power quality in grid-connected hybrid system with power monitoring and control based on internet of things approach (July 20, 2022). Electrical Engineering & Electromechanics, (4), 44–50, 2022.

[22] Dr.M Manikandan, Sanepalle Gopal Reddy, S Ganapathy, ,2022 Three Phase Four Switch Inverter based DVR for power quality improvement with optimized CSA approach,IEEE Access, Institute of Electrical and Electronics Engineers (IEEE), 05 July 2022 10.1109/ACCESS.2022.3188629

[23] .Manikandan, M, Praveen Kumar, T. and Ganapathy, S. and., Improvement of Voltage Stability for Grid Connected Solar Photovoltaic Systems Using Static Synchronous Compensator With Recurrent Neural Network (April 18, 2022). Electrical Engineering & Electromechanics, (2), 69–77, 2022. https://doi.org/10.20998/2074-272X.2022.2.10, Available at SSRN: https://ssrn.com/abstract=4091663

[24] Dr.Manikandan Sathish Ch, Chidambram I.A "Reactive Power Compensation in a Hybrid Renewable Energy System through Fuzzy Based Boost Converter" PROBLEMS of the REGIONAL ENERGETICS 2022, 1(53), DOI: https://doi.org/10.52254/1857-0070.2022.1-53.02

[25] Dr. Manikandan M, Gopal Reddy S., Ganapathy S"Power quality improvement in distribution system based on dynamic voltage restorer using PI tuned fuzzy logic controller" Electrical Engineering & Electromechanics, 2022, no. 1, pp. 44-50. doi: https://doi.org/10.20998/2074-272X.2022.1.06 (WOS-ESCI)- (Scopus)

[26] Dr. M. Manikandan and Vishwaprakash Babu,2021 Power Quality Enhancement using Dynamic Voltage Restorer (DVR) Based Predictive Space Vector Transformation (PSVT) with Proportional Resonant (PR)-controller,IEEE Access, Institute of Electrical and Electronics Engineers (IEEE), 17 November 2021 DOI: 10.1109/ACCESS.2021.3129096

[27] Dr. M. Manikandan and T PraveenKumar,2021, Voltage Sag Compensation and Harmonic Reduction Using STATCOM based DVR with Phase Alternate Fuzzy Controller for Distribution Grid, Design Engineering, Volume 8, Issue 9 PP: 13026 – 13037, 2021

[28] Dr. M. Manikandan and Vishwaprakash Babu,2021,Cascaded Fuzzy Logic Control of PV Fed DVR for Power Distribution Systems, Design Engineering, Volume 8, Issue 9 PP: 8890–8900, 2021

[29] M.Manikandan I.A.Chidambaram, "Smart Fuzzy Control Based Hybrid PV-Wind Energy Generation System" Meterials:proceeding,26th july 2021 article in press

[30] Dr. M. Manikandan and Vishwaprakash Babu, 2021 A Novel Intrinsic SPACE Vector Transformation Based Solar Fed Dynamic Voltage Restorer For Power Quality Improvement In Distribution System, Journal of Ambient Intelligence and Humanized Computing, Volume 10, Issue 9, Page no.7102-7114 & 2021

[31] Dr. M. Manikandan and Vishwaprakash Babu,2020 Voltage Sag /Swell Compensation Using Solar Photovoltaic Inverter based Dynamic Voltage Restorer (SPVI-DVR), Journal of Green Engineering (JGE), Volume 10, Issue 9, Page no.7102-7114 & 2020

[32] Dr. M. Manikandan and Vishwaprakash Babu, 2019 A Novel Integration of Solar Fed Dynamic Voltage Restorer for Compensating Sag and Swell Voltage in Distribution System Using Enhanced Space Vector Pulse Width Modulation (ESVPWM) Universal Journal of Electrical and Electronic Engineering 6 (5), 329-350